an amount insufficient to be resolved in the experimental spectra given the inherent width of the transitions (20 cm^{-1}). The comparison with the experimental spectra (Fig. 3, A and B) leads to an assignment of BW_8(I) as BW_8 (cubic S_4) and BW_8(II) as BW_8(cubic D_{2d}). Weaker transitions, due to the symmetric-stretch double-donor transitions, are observed between 3450 and 3520 cm^{-1}, also consistent with the predictions of the calculations.

The change induced by benzene in the single-donor region is larger than that in the double-donor transitions. In the absence of benzene, the single-donor normal modes are delocalized over all four single-donor OH groups in the cube. By symmetry, all of the single-donor IR intensity is concentrated in a single transition in $W_8(D_{2d})$ and in a doubly degenerate set of transitions in $W_8(S_4)$. Because the binding of benzene to the W_8 cubes occurs through the free OH group of one of the single-donor water molecules, the single-donor normal modes calculated for BW_8(cubic D_{2d}) and BW_8(cubic S_4) become partially localized, thereby redistributing the single-donor OH stretch intensity amongst the normal modes.

For both BW_8 isomers, the experimental spectra in the single-donor region have three resolved, approximately equally spaced transitions. The calculated spectrum of $BW_8(S_4)$ (Fig. 3C) reproduces both the spacing and the intensity profile of the experimental spectrum in this region (Fig. 3A). For $BW_8(D_{2d})$, the spacing between transitions is correct, but the relative intensities of the two highest frequency transitions is reversed (Fig. 3, B and D). This discrepancy may reflect a deficiency in the atomic basis sets.

The OH stretch IR spectra, especially in the double-donor region near 3550 cm^{-1}, provide unique spectral signatures of these cubic structures, distinguishing them from the bicoordinated cyclic structures of the water trimer to pentamer, and the tetracoordinated water molecules found in liquid water and ice.

It is hoped that the present data will stimulate further structural characterization of the D_{2d} and S_4 cubic structures of W_8. Despite their near identical rotational constants (Table 2), the rotational levels of the D_{2d} and S_4 structures will have different nuclear-spin statistical weights, which could be used in rotationally resolved spectra to distinguish the two structures. The cubic isomers may also differ in their hydrogen tunneling behavior.

REFERENCES AND NOTES

1. C. J. Tsai and K. D. Jordan, *J. Chem. Phys.* **95**, 3850 (1991).
2. C. Lee, H. Chen, G. Fitzgerald, *ibid.* **102**, 1266 (1995); R. Knochenmuss and S. Leutwyler, *ibid.* **96**, 5233 (1992); D. A. Estrin, L. Paglieri, G. Corongui, E. Clementi, *J. Phys. Chem.* **100**, 8701 (1996).
3. K. S. Kim, M. Dupuis, G. C. Lie, E. Clementi, *Chem. Phys. Lett.* **131**, 451 (1986); G. Brink and L. Glasser, *J. Phys. Chem.* **88**, 3412 (1984).
4. C. J. Tsai and K. D. Jordan, *J. Phys. Chem.* **97**, 5208 (1993).
5. D. J. Wales and I. Ohmine, *J. Chem. Phys.* **98**, 7245 (1993).
6. B. Rowland *et al.*, *ibid.* **102**, 8328 (1995).
7. Q. Du, R. Superfine, E. Freysz, Y. R. Shen, *Phys. Rev. Lett.* **70**, 2313 (1993).
8. G. C. Pimentel and A. L. McClellan, *The Hydrogen Bond* (Freeman, San Francisco, 1960).
9. F. Huisken, M. Kaloudis, A. Kulcke, *J. Chem. Phys.* **104**, 17 (1996), and references therein.
10. R. N. Pribble and T. S. Zwier, *Science* **265**, 75 (1994); *Discuss. Faraday Soc.* **97**, 229 (1994).
11. R. N. Pribble, A. W. Garrett, K. Haber, T. S. Zwier, *J. Chem. Phys.* **103**, 531 (1995).
12. S. Y. Fredericks, K. D. Jordan, T. S. Zwier, *J. Phys. Chem.* **100**, 7810 (1996).
13. T. S. Zwier, *Annu. Rev. Phys. Chem.* **47**, 205 (1996).
14. A. W. Garrett and T. S. Zwier, *J. Chem. Phys.* **96**, 3402 (1992).
15. A. J. Gotch and T. S. Zwier, *ibid.*, p. 3388.
16. A. E. W. Knight, C. S. Parmenter, M. W. Schuyler, *J. Am. Chem. Soc.* **97**, 1993 (1975).
17. R. N. Pribble, C. Gruenloh, T. S. Zwier, *Chem. Phys. Lett.* **262**, 627 (1996).
18. The Becke3LYP functional combines Becke's hybrid exchange functional [A. D. Becke, *J. Chem. Phys.* **98**, 5648 (1993)] and the LYP correlation functional [C. Lee, W. Yang, R. G. Parr, *Phys. Rev. B* **37**, 785 (1988)], with the weights of the various terms in the functional being the default values in Gaussian 94. The 6-31 +G[d,p] basis set combines the 6-31 +G basis set with the diffuse polarization functions from the aug-cc-pVDZ set [R. A. Kendall, T. H. Dunning Jr., R. J. Harrison, *J. Chem. Phys.* **96**, 6796 (1992)].
19. T. Clark, J. Chandrasekhar, G. W. Spitznagel, P. v. R Schleyer, *J. Comp. Chem.* **4**, 294 (1983); W. J. Hehre, R. Ditchfield, J. A. Pople, *J. Chem. Phys.* **56**, 2257 (1972); M. J. Frisch, J. A. Pople, J. S. Binkley, *ibid.* **80**, 3265 (1984).
20. K. Kim and K. D. Jordan, *J. Phys. Chem.* **98**, 10089 (1994).
21. Previous work (*12, 20, 22*) has demonstrated that DFT calculations using the Becke3LYP functional faithfully reproduce the trends in the OH stretch spectra of water and benzene-water clusters. The major deficiency of such calculations is an exaggeration of the magnitude of the shifts of the single-donor OH stretch frequencies.
22. J. E. Del Bene, W. B. Person, K. Szczepaniak, *J. Phys. Chem.* **99**, 10705 (1995); S. S. Xantheas, *J. Chem. Phys.* **102**, 4595 (1995).
23. Gaussian 94 (Rev. G); M. J. Frisch *et al.*, Gaussian Inc., Pittsburgh, PA (1995).
24. A table of the calculated vibrational frequencies, frequency shifts, and IR intensities for $W_8(D_{2d})$, $W_8(S_4)$, $BW_8(D_{2d})$, and $BW_8(S_4)$ is available on the World Wide Web at http://www.pitt.edu/~jordan/science_article/BW8/table

25. We gratefully acknowledge NSF for support of this research from grants CHE-9404716 and CHE-9422210. We thank C. Sosa of Silicon Graphics and Cray Research for assistance with some of the calculations.

7 February 1997; accepted 7 April 1997

Atomic Selectivity in the Chemisorption of ICl (Iodochloride) on Silicon Surfaces

Yong Liu, Denis P. Masson, Andrew C. Kummel*

When ICl adsorbs on a clean silicon (111)-(7×7) surface, the reaction is chemically selective. This process has been studied with the use of scanning tunneling microscopy and Auger spectroscopy. The dominant mechanism is the formation of silicon monoiodide by abstraction and the ejection of the chlorine atoms back into the gas phase. This pathway is not only chemically selective but also the least exothermic of all the possible reaction mechanisms. Although atomic chemical selectivity in gas-phase reactions is quite common, atomic chemical selectivity is unexpected in gas-surface reactions on clean surfaces because of the high density of reactive sites.

The gas-phase reaction of ICl molecules with deuterium is chemically selective; the yield of DI exceeds DCl by a factor of at least 3 despite the much lower exothermicity for forming DI (84 kJ mol^{-1}) compared with DCl (218 kJ mol^{-1}) (*1*). From a dynamical point of view, a fundamentally interesting question is whether such a chemical selectivity observed in gas-phase reactions can exist in molecule-surface interactions. For the chemisorption of ICl onto the Si(111)-(7×7) surface, there are three possible competitive reaction channels: dissociative adsorption (Eq. 1), chlorine-selective abstraction (Eq. 2), and iodine-selective abstraction (Eq. 3).

$$\text{I–Cl(g)} + 2\text{Si} \rightarrow \text{Si–I} + \text{Si–Cl}$$
$$\Delta E = -5.59\text{eV} \quad (1)$$
$$\text{I–Cl(g)} + \text{Si} \rightarrow \text{Si–Cl} + \text{I(g)}$$
$$\Delta E = -2.55\text{eV} \quad (2)$$
$$\text{I–Cl(g)} + \text{Si} \rightarrow \text{Si–I} + \text{Cl(g)}$$
$$\Delta E = -0.86\text{eV} \quad (3)$$

In dissociative adsorption, the chemical bond of an ICl molecule breaks, so that the I and Cl atoms separately form chemical bonds with the surface. In abstractive adsorption, one halogen atom (X) in an ICl molecule forms a chemical bond with the surface and the other is ejected into the gas

Department of Chemistry, 0358, University of California at San Diego, 9500 Gilman Drive, La Jolla, CA 92093, USA.

*To whom correspondence should be addressed.

phase (*2*, *3*). We have used scanning tunneling microscopy (STM) and surface elemental analysis to determine (i) the relative importance of dissociative chemisorption versus abstractive chemisorption and (ii) the branching ratio between I-selective and Cl-selective abstraction. The dominant reaction channel is the least exothermic one, I-selective abstraction. Therefore, ICl reacts with the surface to produce an I-rich adsorbate layer, not a stoichiometric adsorbate layer. Although atomic selectivity in gas-phase reactions is common, we have observed atomic selectivity in a gas-surface reaction in which all the reaction products form stable adsorbates; a phenomenon we call atomically selective chemisorption.

A clean Si(111)-(7×7) surface is composed of periodically arranged rhombohedral 7×7 unit cells with 46.56 Å long diagonals and 26.88 Å short diagonals (*4*). At low coverage, the molecular halogens only react with the topmost silicon "adatom" layer (*5*). The adatoms are arranged in a diamond configuration of two triangular subunits. At the vertices of the diamond are the "corner holes"; at these locations, there are no Si atoms in the first or second layers. Each of the 12 adatoms has a partially filled dangling bond directed along the surface normal that is both reactive and readily imaged (Fig. 1A) by STM. Abstractive and dissociative adsorption onto the dangling bonds has been directly observed in STM topographic images for the chemisorption of F_2, Cl_2, and Br_2 on the Si(111)-(7×7) surface (*6*–*8*).

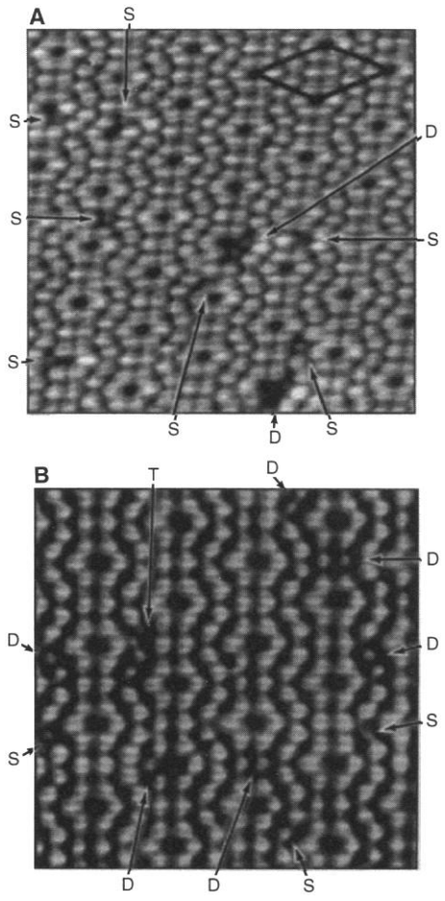

Fig. 1. Empty-state STM topographic images of the Si(111)-(7×7) surfaces dosed with (**A**) 1.2-eV ICl (+2.0-V bias, 0.48-nA tunneling current) and (**B**) 0.89-eV Br_2 (+0.6 V and 0.24 nA). Isolated single, paired (double), and trimer reacted sites are labeled as S, D, and T, respectively. An unreacted clean (7×7) unit cell of Si(111) is outlined in the upper-right corner of (A).

In our experiments, the I-selective chemisorption of monoenergetic ICl was investigated with the use of monoenergetic supersonic molecular beams. Although the ICl was translationally energetic (0.2 to 1.2 eV), it was rotationally cold (~2 K), thus facilitating rotation of the molecule by an anisotropic gas-surface interaction and probably accentuating the atomically selective chemisorption. Briefly, a three-stage differentially pumped, pulsed supersonic molecular-beam source was coupled to an ultrahigh-vacuum chamber (*7*). The ICl molecules were expanded at room temperature and a stagnation pressure of 2.8×10^5 Pa through a pulsed valve. The kinetic energies of ICl molecules seeded in He or Ar beams were determined by time-of-flight measurements to be 1.2 and 0.2 eV, respectively. Great care was taken to ensure that there were minimal impurity gases (particularly <0.1% Cl_2 and <2% I_2) in the beams before dosing. A cylindrical mirror–analyzer Auger electron spectrometer was used to measure the absolute ratio of Cl to I on the Si(111)-(7×7) surfaces after exposure to monoenergetic ICl molecules. A STM instrument (Park Scientific) in the ultrahigh-vacuum chamber was used to record the types of adsorption sites and thus differentiate between abstractive and dissociative chemisorption..

An STM topographic image of a Si(111)-(7×7) surface after dosing with 1.2-eV ICl molecules at room temperature (Fig. 1A) shows that the unreacted Si adatoms appear as bright spots and the corner holes as dark spots. The reacted Si adatoms appear as dim spots because their dangling bonds have been eliminated by the newly formed Si–Cl or Si–I chemical bonds. By counting these dim spots, the total coverage of reacted adatoms is readily determined to be 0.028 ± 0.002 monolayer (ML). These dim spots are either silicon monoiodide (Si–I) or silicon monochloride (Si–Cl) surface species and cannot be distinguished from each other in STM topographic images. The STM images can also be used to determine the relative probability of abstractive versus dissociative chemisorption. In dissociative chemisorption of a diatomic halogen on Si(111)-(7×7), the halogen atoms bind to nearest neighbor Si adatoms, and thus, a pair of dim atoms is observed in STM. Conversely, in abstractive chemisorption, only one of the halogen atoms binds to the surface, and only an isolated single reacted adatom is observed in STM (*6*).

In Fig. 1A, there are seven isolated reacted sites (labeled "S") and only two paired reacted sites (labeled "D," for dimers). Because the bonding between Si and halogen atoms is covalent in nature, the diffusive energy barriers for Cl and I atoms on the Si(111)-(7×7) surface are sufficiently high to prevent them from diffusing at room temperature. Therefore, the seven isolated dim sites are all identified as Si–Cl or Si–I formed by abstractive adsorption. Each of the paired sites (labeled as "D") in Fig. 1A most likely consists of one Si–Cl and one Si–I species formed by a dissociative adsorption event. Although paired dim spots might be formed by the coincidence of two separate abstractive adsorption events, the probability of such a coincidence is negligibly small at a total coverage of 0.028 ML. The bottom paired site might also consist of a single silicon monohalide(Si–X) plus a defect because missing Si adatoms (defects) primarily appear as dark as corner holes. Although there is some uncertainty regarding the origin of the two "D" sites, isolated Si–X species dominate the entire STM image, indicating that the adsorption of ICl molecules on the Si(111)-(7×7) surface proceeds predominantly through the abstractive adsorption mechanism.

The percentages of Si–X species located in isolated single, paired, and larger sites have been plotted in Fig. 2. No distinction has been made between Si–Cl and Si–I sites. For an ICl incident energy of 1.2 eV, the adsorbate size distributions were obtained from STM images with total coverages of 0.056 ± 0.002 ML covering 340 unit cells, whereas for an incident energy of 0.2 eV, a coverage of 0.052 ML ± 0.002 ML and 312 unit cells were used. Figure 2 shows that ~58% of the adsorbed halogen atoms formed isolated single sites, 28% formed paired sites, and 14% formed larger sites. Moreover, the incident energy of ICl had little effect on the adsorbate size distribution. To calculate the ratio of abstraction to dissociative chemisorption, we performed a Monte Carlo simulation in which single and paired sites were randomly placed on 7×7 unit cells until the experimental total coverage was reached. The abstraction probability was optimized until the size distribution matched the experimental data.

Using this technique, we determined the probability of abstractive adsorption for ICl on the Si(111)-(7×7) surface to be 0.82 ± 0.03, whereas the dissociation probability is only 0.18 ± 0.03.

The Br_2 molecule has a bond length (2.29 Å) and a bond strength (2.01 eV) similar to those of ICl. However, empty-state STM images for the Si(111)-(7×7) surface dosed with 0.89-eV Br_2 molecules (Fig. 1B) were dominated by dimer sites instead of isolated single sites. At a total coverage of 0.060 ± 0.002 ML, only 23% of the Br atoms formed isolated single sites, 54% formed paired sites, and 23% formed larger sites (Fig. 2). This yields a probability of just 0.43 ± 0.03 for the abstractive adsorption with our Monte Carlo simulation.

Auger electron spectroscopy (AES) has been used to quantitatively determine the ratio of Cl atoms to I atoms on the Si(111)-(7×7) surface after exposures to monoenergetic ICl molecules. In the AES measurements, an unfocused electron beam (3 kV) of low flux was used to minimize the electron-stimulated desorption of Cl from the Si(111)-(7×7) surface so that there was no discernible decrease in the Cl or I AES signals during the 5 min of electron bombardment. The relative AES sensitivity of Cl to I was assumed to be 3.3:1 (9). We checked this sensitivity by dosing the surface continuously to create 300 K etching. Under these conditions, ICl adsorbs by means of an extrinsic precursor, and thus, we expect the Cl to I ratio to be 1:1. Our experimentally measured value of the Cl/I ratio at saturation coverage is within 15% of unity (Fig. 3), which confirms the value of our Auger sensitivity factors. The Cl/I ratio did reach unity because molecular-beam dosing has a low flux, and thus, the surface was insufficiently etched to remove the I-rich adsorbate layer formed at low coverage. Therefore, our relative AES sensitivity was accurate to within ~10%. Surprisingly, the absolute Cl to I ratio was only 0.3 at low total coverage and increased steadily to 1 as the total coverage increased (Fig. 3). The Cl to I ratio of 0.3 at low total coverage was significantly lower than the stoichiometric ratio of 1 for an ICl molecule. This decrease is direct experimental evidence that the least exothermic reaction, I-selective abstraction, dominates the adsorption of ICl at the clean Si(111)-(7×7) surface over the energetically favored Cl-selective abstraction and dissociative-chemisorption reactions.

To verify the excess of I on the surface, we performed mass-resolved flash desorption experiments in which the Si(111)-(7×7) surfaces predosed with ICl were flashed to ~1300 K. The quadruple mass spectrometer signals from desorption products containing Cl and I ($SiCl_2^+$ and I^+) were simultaneously recorded in real time. The parent molecule of $SiCl_2^+$ is $SiCl_2$, but the parent molecule of I^+ is either SiI_2 or SiICl, and thus, the chemical selectivity measured with flash desorption should be slightly less than that measured using AES. The sensitivities were calibrated by assuming that the ratio of Cl to I on the surface at the highest coverage was 1:1 because under these conditions there is 300 K continuous etching and ICl absorbs by means of an extrinsic precursor. The flash desorption results show that at low coverage, the surface is enriched in I compared to Cl by a factor of 2.1 ± 0.3, and the AES results gave a ratio of 2.8 ± 0.6. These ratios confirm that the Si(111)-(7×7) surface selectively abstracts I atoms from ICl molecules and ejects Cl atoms into the gas phase.

The atomically selective chemisorption exhibited by ICl during abstractive adsorption onto the Si(111)-(7×7) surface may occur because I-end–first collisions of ICl are more reactive to Si adatoms than Cl-end–first collisions. If this asymmetry is the case, the initial sticking probability of ICl should be <0.5 because the ICl molecules are oriented isotropically before hitting the Si(111)-(7×7) surface. By using the beam-reflection technique (*10*), the initial sticking probabilities of 0.2- and 1.2-eV ICl were measured to be 0.89 ± 0.07 over the surface temperature range of 293 to 970 K. Because the measured initial sticking probabilities are significantly greater than 0.5, the chemical selectivity cannot be explained by assuming stereoselectivity for the abstractive adsorption of ICl.

To reconcile the dominant I-selective abstraction with the high initial sticking probability for ICl on the Si(111)-(7×7) surface, we propose that the surface reorients the ICl molecules into an I-end–first configuration during gas-surface collisions (Fig. 4). As a rotationally cold (~2 K) ICl molecule from the molecular beam approaches the surface, both physical and chemical interactions between the ICl and the Si(111)-(7×7) surface will orient the ICl into an I-end–first orientation. Each I-end–first collision preferentially forms a short-lived transition state that contains a central I atom partially bonded to both a Cl atom and a Si adatom, that is, Si-I-Cl(s). As the reaction proceeds, the I–Cl bond of the Si-I-Cl(s) transition state breaks, the Cl atom is ejected into the gas, and a chemisorbed silicon monoiodide Si–I(s) is formed. Because the I-end–first orientation of ICl prohibits the formation of a Si-Cl-I(s) transition state, it is impossible for the Si(111)-(7×7) surface to abstract a Cl atom from an

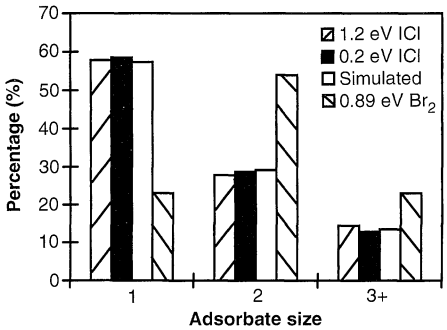

Fig. 2. Experimental adsorbate size distributions for the Si(111)-(7×7) surfaces dosed at room temperature with 1.2-eV ICl, 0.2-eV ICl, and 0.89-eV Br_2 molecules, with total coverages of 0.056, 0.052, and 0.060 ± 0.002 ML, respectively. The fitted adsorbate size distribution was generated by a Monte Carlo simulation using a defect coverage of 0.005 ML, a halogen coverage of 0.051 ML, and a 82% probability for the abstractive adsorption of ICl on the Si(111)-(7×7) surface.

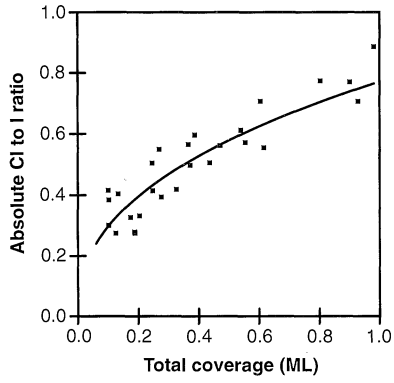

Fig. 3. Absolute Cl to I ratio versus total halogen coverage for dosing of 1.2-eV ICl molecules onto 300 K Si(111)-(7×7). The absolute Cl to I ratios were calculated from the Auger electron signals of Cl-LMM (181 eV) and I-MNN (511 eV) and a relative sensitivity ratio of Cl/I = 3.3 ± 0.3. In this figure, the coverage is the ratio of halogens to silicon adatoms and was calibrated at 0.10 ML by STM and at 1.0 ML by a molecular beam saturation dose of ~25 Langmuirs. The coverage of 1 ML corresponds to an AES halogen/silicon ratio of 0.30 ± 0.03 .

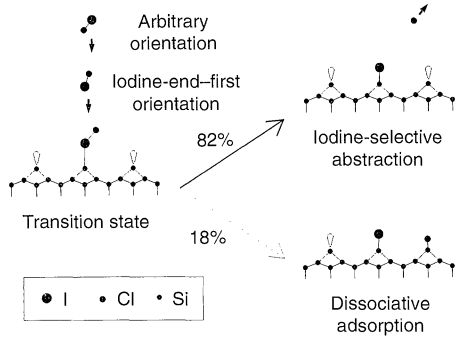

Fig. 4. Schematic of the reaction mechanisms proposed for the adsorption of monoenergetic ICl molecules on the Si(111)-(7×7) surfaces.

ICl and eject an I atom back to the gas phase (Cl-selective abstraction) despite the much larger exothermicity for the formation of Si–Cl(s) + I than Si–I(s) + Cl.

The reorientation by the surface would also explain the higher abstraction ratio for ICl over that for Br_2. An end-on geometry has been calculated to favor abstraction over dissociation for halogens on semiconductor and metal surfaces because this geometry places the terminal halogen far from the surface in an optimal position for abstraction (*2*, *11*). Although molecules in the molecular beam usually have a nearly side-on or tilted orientation, reorientation by the surface should place a large fraction of the ICl into an end-on geometry and thus increase abstraction.

We propose that the orientation of ICl into I-end–first configuration results from the higher polarizability of I compared to Cl and the asymmetric molecular bonding associated with ICl. Because Cl is much more electronegative than I, the bonding σ_z and $\pi_{x,y}$ orbitals predominantly consist of Cl 3*p* orbitals, whereas the antibonding σ_z* and $\pi_{x,y}$* orbitals predominantly consist of I 5*p* orbitals. The highest occupied molecular orbital (HOMO) is mainly concentrated at the I atom of an ICl molecule; thus, the I end is both more polarizable and more reactive than the Cl end. This difference was confirmed by Hartree-Fock molecular orbital calculations made using the SpartanPlus program (*12*) which show that the effective radius of the π*-orbital wave function is 70% greater on the I atom than on the Cl atom. Conversely, there is only 10% difference in the effective radius of the probability density of the entire valence shell between the I and the Cl atoms. Therefore, we suggest that when an ICl molecule approaches a Si adatom on the Si(111)-(7×7) surface, the interaction of an ICl $\pi_{x,y}$* antibond (HOMO) with the partially filled Si dangling bond results in greater attraction to the I end than the Cl end of the ICl molecule. This selection is the driving force for the I-end–first orientation of ICl before reaction and ultimately causes chemical selectivity for the reaction of ICl with the Si(111)-(7×7) surface. This same molecular-orbital argument was used to explain the chemical selectivity of the D + ICl → DI + Cl gas-phase reaction (*1*). Reorientation of NO (*13*) by Ag(111) or Pt(111) and of H_2 by W(100) (*14*) or Pd(100) (*15*) is denoted as rotational steering and has been observed in theoretical simulations. Therefore, the reorientation of molecules by surfaces may be a general phenomenon and is probably the dynamic mechanism responsible for this example of atomically selective chemisorption, the selective abstraction of I from ICl by Si(111)-(7×7).

REFERENCES AND NOTES

1. J. C. McDonald, P. R. LeBreton, Y. T. Lee, D. R. Herschback, *J. Chem. Phys.* **56**, 769 (1972).
2. L. E. Carter, S. Khodabanedeh, P. C. Weakliem, E. A. Carter, *ibid.* **100**, 2277 (1994).
3. Y. L. Li *et al.*, *Phys. Rev. Lett.* **74**, 2603 (1995).
4. K. Takayanagi, Y. Tanishiro, M. Takahashi, S. Takahashi, *J. Vac. Sci. Technol. A* **3**, 1502 (1985).
5. D. Purdie *et al.*, *J. Phys.* **3**, 7751 (1991); J. J. Bolland and J. S. Villarrubia, *Phys. Rev. B.* **41**, 9865 (1990).
6. J. A. Jensen, C. Yan, A. C. Kummel, *Science* **267**, 493 (1995).
7. C. Yan, J. A. Jensen, A. C. Kummel, *J. Chem. Phys.* **102**, 3381 (1995).
8. J. A. Jensen, C. Yan, A. C. Kummel, *Phys. Rev. Lett.* **76**, 1388 (1996).
9. P. W. Palmberg, G. E. Riach, R. E. Weber, N. C. MacDonald, *Handbook of Auger Electron Spectroscopy* (Physical Electronics, Edina, MN, 1972).
10. D. A. King and M. G. Wells, *Surf. Sci.* **29**, 454 (1972).
11. J. Stromquist, L. Hellberg, B. Kasemo, B. I. Lundqvist, *ibid.* **352**, 435 (1996).
12. SpartanPlus; Wavefunction, Irvine, CA.
13. C. W. Mulhausen, L. R. Williams, J. C. Tully, *J. Chem. Phys.* **83**, 2594 (1985); D. Lemoine, *ibid.* **101**, 4350 (1994); B. Pouilly, J. M. Roobe, D. Lemoine, *J. Phys. Condens. Matter* **6**, 9689 (1994).
14. M. Kay, G. R. Darling, S. Holloway, J. A. White, D. M. Bird, *Chem. Phys. Lett.* **245**, 311 (1995).
15. A. Gross, S. Wilke, M. Scheffler, *Phys. Rev. Lett.* **75**, 2718 (1995).

16. We thank NSF (grant DMR-9307259) and the U.S. Air Force Office of Scientific Research (grant 94-10075) for funding this work, A. Komrowski and K. Pettus for helpful assistance in the experiments, and P. Taylor of the Univ. of California at San Diego Supercomputer Center for performing the molecular orbital calculations.

19 February 1997; accepted 11 April 1997

Differential Effects of Cytolytic T Cell Subsets on Intracellular Infection

Steffen Stenger, Richard J. Mazzaccaro, Koichi Uyemura, Sungae Cho, Peter F. Barnes, Jean-Pierre Rosat, Alessandro Sette, Michael B. Brenner, Steven A. Porcelli, Barry R. Bloom, Robert L. Modlin*

In analyzing mechanisms of protection against intracellular infections, a series of human CD1-restricted T cell lines of two distinct phenotypes were derived. Both $CD4^-CD8^-$ (double-negative) T cells and $CD8^+$ T cells efficiently lysed macrophages infected with *Mycobacterium tuberculosis*. The cytotoxicity of $CD4^-CD8^-$ T cells was mediated by Fas-FasL interaction and had no effect on the viability of the mycobacteria. The $CD8^+$ T cells lysed infected macrophages by a Fas-independent, granule-dependent mechanism that resulted in killing of bacteria. These data indicate that two phenotypically distinct subsets of human cytolytic T lymphocytes use different mechanisms to kill infected cells and contribute in different ways to host defense against intracellular infection.

Effective immunity to intracellular bacterial infection often requires the lysis of infected cells as well as killing of the invading pathogen. A possible role for cytolytic T lymphocytes (CTLs) in protection against *M. tuberculosis* has been suggested by experiments in mice bearing a disruption in the β_2-microglobulin gene. These mice are unable to express major histocompatibility complex (MHC) class I or class I–like molecules or to generate CTLs and were shown to be highly susceptible to infection (*1*). Despite numerous studies of $CD4^+$ T cell responses and cytokine production in tuberculosis, there remain only a few reports of $CD8^+$ CTLs that recognize mycobacterial antigens (*2*). This paradox led us to investigate whether other antigen-presenting systems could be essential for generation of *M. tuberculosis*–specific CTLs. CD1 is an MHC-like surface molecule with a unique ability to process and present nonpeptide antigens to T cells, including mycobacterial lipids (*3*, *4*). We examined whether CD1-restricted CTLs have the capacity to recognize and lyse *M. tuberculosis*–infected macrophages.

CD1-restricted T cells were derived from patients with active tuberculosis as well as healthy donors (*5*). All of these T cell lines recognized *M. tuberculosis* lipid and lipoglycan antigens in a CD1b-restricted manner as assessed by antigen-

S. Stenger, K. Uyemura, S. Cho, R. L. Modlin, Division of Dermatology and Department of Microbiology and Immunology, University of California Los Angeles School of Medicine, Los Angeles, CA 90095, USA.
R. J. Mazzaccaro and B. R. Bloom, Howard Hughes Medical Institute, Albert Einstein College of Medicine, Bronx, NY 10461, USA.
P. F. Barnes, Department of Medicine, University of Southern California School of Medicine, Los Angeles, CA 90033, USA.
J.-P. Rosat, M. B. Brenner, S. A. Porcelli, Department of Rheumatology and Immunology, Brigham and Women's Hospital, Boston, MA 02115, USA.
A. Sette, Department of Immunology, Cytel Corporation, San Diego, CA 92121, USA.

*To whom correspondence should be addressed. E-mail: rmodlin@medicine.medsch.ucla.edu